Thirteenth International Conference on Domain Decomposition Methods
Editors: N. Debit, M.Garbey, R. Hoppe, J. Périaux, D. Keyes, Y. Kuznetsov

10 Cartesian and Curvilinear Grid Methods for Multi-domain, Moving Boundary Problems

W. Shyy[1] M. Francois[2] H.S. Udaykumar[3]

Introduction

A variety of physical phenomena involve the coupling of evolution of multiple materials with boundaries that move, deform or evolve in time. Examples include the deformation of drops, bubbles, liquid free surfaces, phase boundaries in solidification and vaporization, fluid-structure interaction problems at the large scale such as in aeroelasticity and in the small scale such in biomechanics, and a whole host of other interesting phenomena. These problems are challenging due to the complexity associated with the often severely deformed boundaries, multiple time and length scales, and the nonlinearity resulting from the coupling of the interface dynamics with the dynamics of the material. Ideally one would like to track the moving boundary as a sharp front (allowing discontinuities in quantities such as stress and energy across the interface) without smearing the information at the front. Also, one would like to solve the field equations within each region separated by the interfaces with satisfactory accuracy. If the interfaces become multiply-connected, it is desirable to follow the evolution of the interfaces through such topological changes. Numerous techniques exist for tracking arbitrarily shaped moving interfaces, each with its own strengths and weaknesses [Cra84, FR89, SURS96]. These techniques may be classified under two main categories: (a) surface tracking or predominantly Lagrangian methods [FZP$^+$93, SS95, SS96] and (b) volume tracking or Eulerian methods [HN81, AP91]. The main features of the two types are presented in Figure 1. We offer the following comments to contrast the relative characteristics among different approaches.

a. Interface Definition

The Lagrangian methods maintain the interface as a discontinuity and explicitly track its evolution. If detailed information regarding the interface location is desired, Eulerian methods may need elaborate procedures to deduce the interface location based on the volume fraction information, and uncertainty corresponding to one grid cell is unavoidable [AP91, HN81, SZ99]. In the Lagrangian case, the interface can be tracked as a (n-1)-dimensional entity for a n-dimensional space [DS85, GGL$^+$88, WM86]. No modeling is necessary to define the interface or its effect on the flow field. In the case of Eulerian schemes, modeling or solution of additional equations is required to obtain information regarding phase fractions or other functions yielding information in the two-phase regions.

[1]Department of Aerospace Engineering, Mechanics and Engineering Science, University of Florida, wss@aero.ufl.edu
[2]Department of Aerospace Engineering, Mechanics and Engineering Science, University of Florida, francoim@aero.ufl.edu
[3]Department of Mechanical Engineering, University of Iowa.

b. Interfacial Boundary Conditions

In the Lagrangian methods, boundary conditions can be applied at the exact location of the interface since the interface position is explicitly known at each instant. In the Eulerian methods, the boundary conditions are manipulated to appear in the governing transport equations [BKZ92]. This leads to the smearing of boundary information.

c. Discretization of the Domain

In the Lagrangian methods, the grid adapts to the interface and hence grid rearrangement and motion terms have to be incorporated. When the interface begins to distort, the grid needs to be regenerated each time. The resulting grid on which the field variables are computed may be skewed and unevenly distributed, thus influencing the accuracy of the field solver. The Eulerian methods have an advantage in this regard since the computations are performed on a fixed grid, hence obviating the need for grid rearrangement. However, when the interface is arbitrarily shaped, improved resolution in desired regions is difficult to obtain, unless complicated local refinements are adopted. In the Lagrangian method a set of governing equations needs to be solved for each different material and region, whereas in an Eulerian method only a single set of equations with appropriate source terms is solved for the entire domain.

d. Movement and Deformation of the Interface

Lagrangian methods have so far experienced difficulty in handling topological changes, mainly due to the breakdown of the structured grid arrangement and the need for redistribution of field information in the vicinity of the interface for unstructured grid methods [WM86]. On the other hand, in Eulerian methods mergers and fragmentations are taken care of automatically, merely by updating the values of the phase fraction. However, the detailed physical features involved during such events may not be fully resolved due to the smearing of information as mentioned above. The choice of moving boundary method from the general categories above depends to a large extent on its appropriateness of the physical problem chosen. In the following, we highlight recent efforts in developing computational techniques for treating moving boundary problems. Both moving and fixed grid methods will be considered. To aid the discussion, for the fixed grid method, we use the impact dynamics, and for the moving grid method, we use the soft contact lens dynamics to highlight the solution characteristics.

A Fixed-grid, Sharp-interface Method for Multiple Moving Boundaries: Impact Dynamics

The dynamics of impact between materials is characterized by large deformation and short time scales. Wave propagation in the impacting media is highly nonlinear, and involves localized phenomena such as shear bands, crack propagation, and wave refraction [Mey94]. These problems are typically challenging to solve because, in contrast to conventional structural dynamics problems, the deviatoric and pressure terms in the stress tensors are both important and need to be modeled separately. In contrast to conventional fluid dynamics problems, the stress and strain fields are related through nonlinear elasto-plastic yield surfaces, the models for which must be included in the governing equations. Furthermore,

the interface between materials experiences not only fast motion, but also large variations in shape. In this section we summarize a numerical solution technique progressively developed in [SURS96, USR96, UKSTST97, UMS99, UTS+00, YMUS99] for the simulation of high-speed multi-material impact. Of particular interest is the interaction of solid impactors with targets. This problem is important in applications such as munitions-target interactions, automobile collision assessment, geological impact dynamics, and shock processing [Mey94]. Such interactions present the following challenges to numerical simulation techniques:

1. High velocities of impact leading to large deformations of the impactor as well as targets.

2. Nonlinear wave-propagation and the development of shocks in the systems.

3. Modeling of the constitutive properties of materials under intense impact conditions and accurate numerical calculation of the elasto-plastic behaviour described by the models.

4. Phenomena at multiple interfaces (such as impactor-target, target-ambient and impactor-ambient), i.e. both free surface and surface-surface dynamics.

The method adopted falls under the class of combined Eulerian-Lagrangian method. It operates on a fixed Cartesian mesh (the Eulerian part) while the interfaces move through the mesh (the Lagrangian part). The method treats the interfaces as discontinuities without smearing on the mesh, therefore it is a sharp interface method. The advantage of the fixed grid approach is obviously that grid topology remains simple while large distortions of the interface take place. This allows an extension of highly accurate shock-capturing methods (Essentially Non-Oscillatory or ENO [HEOC97, SO88, SO89] in the present case) developed for scalar conservation laws in fixed grid settings to solve moving boundary problems with arbitrarily distorted interfaces. A Cartesian grid ENO formulation suffers little change when applied to the present problem. We now proceed to describe the method in detail.

Interface Tracking Algorithm

The interface is described by interfacial markers defined by the coordinates $X(s)$. The spacing between the markers is maintained at some fraction of the grid spacing h, $0.5h < ds < 1.5h$. The convention adopted is that as one traverses the interface along the arc-length, the material enclosed by the interface lies to the right. This is illustrated in Figure 2. The functions $x(s) = a_x s^2 + b_x s + c_x$ and $y(s) = a_y s^2 + b_y s + c_y$ are generated. The coefficients $a_{x/y}$, $b_{x/y}$ and $c_{x/y}$ at any interfacial point i are obtained by fitting polynomials through the coordinates (x_{i-1}, y_{i-1}), (x_i, y_i) and (x_{i+1}, y_{i+1}). The coefficients $a_{x/y}$, $b_{x/y}$ and $c_{x/y}$ are stored for each marker point. Once the interface has been defined, the information on its relationship with the grid has to be established. There may be several interfaces (henceforth called objects) immersed in the domain. Each of the objects may enclose material with different transport properties. Therefore it is necessary to identify which phase each computational point (i.e. cell center point) lies in. An illustration is shown in Figure 3. The end result of the procedures is the following pieces of information which are required to set up the discretization scheme for the present method: (i) The interfacial cell in which each interface marker lies. (ii) The interfacial marker, which is closest in distance to a computational point. (iii) The material in which each computational point in the mesh lies. (iv) Several geometric details such as the

shape of the resulting cut-cell, the locations where the interface cuts the cell faces and where it intersects the cell center lines (the dotted lines shown in Figure 3). These details of a cell are used in constructing the stencil for each interfacial cell. (v) A list of all interfacial cells. These pieces of information regarding the interface and its relationship to the underlying grid are computed only in a lower-dimensional set of interface cells. In summary, the computational formulation tracks moving boundaries on a fixed underlying grid while striving to achieve the following objectives:

1. The interface is tracked as a discontinuity and boundary conditions of the Dirichlet/Neumann type are applied on the tracked fronts.

2. The discretization to include the embedded boundaries involves simple measures in the vicinity of the interface. Such points are few compared to the overall grid size.

3. Based on truncation error analysis the discretization can be performed so that global second-order accuracy in the field variable can be maintained.

4. The problem of stiffness of the interface evolution in curvature-driven dynamics [HLS94] is surmounted by using an implicit formulation to couple the interface evolution with the field equation.

5. The issue of change of material of a grid point when the boundary crosses over it is dealt with by a simple analogy with purely Lagrangian methods.

This involves redefinition of the stencils in the points adjoining the interface to account for the grid points that have changed phase. The various components of the solution algorithm can easily be extended to 3D. It is demonstrated by [UMS99, YMUS99] that the field calculation is second-order accurate while the position of the phase front is calculated to first-order accuracy. Furthermore, the accuracy estimates hold for the cases where there are property jumps across the interface.

Results and Discussion

2D computations were performed in a square domain of size 1mx1m as illustrated in Figure 4. As shown there the objects were placed some distance apart on the mesh and impact was initiated by prescribing a velocity to one or both interfaces. Initially there is a region of void between the two interfaces. This void disappears at the material- material interface. In Figure 5, we show the impact of a cylinder with a plane surface. Both surfaces are copper and the material properties in the model correspond to that metal. In the figure, we show on the left the contours of velocity magnitude in the impactor and the target along with the velocity vectors in the flow domain. On the right we show contours of equivalent stress. Also shown in each of the figures is the shape of the boundaries of the two materials. As can be seen in these figures there is an abrupt transition in the corners from a material-material interface to a material-void interface for each material. Appropriate governing laws and boundary conditions are discussed in [UTS$^+$00]. Zero-gradient conditions are applied at the sides of the domain assuming that the target has infinite extent in all except the +y direction. Figures 5 (a), (b) and (c) correspond to time instants $2.5\mu s$, $50\mu s$ and $100\mu s$ after impact respectively. The progression of the elasto-plastic waves and the formation of large gradients in the velocity as well stress fields is evident from the figure. At the rim of the impactor, the interfaces are

constantly in collision since the material-void interfaces are being pushed against each other to form material-material interfaces. Thefore the rim of the impact region registers large stress and correspondingly, strain values. Stress waves are propagated into the materials from this point. In Figure 5(c) it can be seen that the velocity field is such as to continuously push the impactor into the target leading to the production of an upswell in the target material around the rim. This is also indicated clearly by the velocity vectors shown. Regions of compression and tension are seen from the contours of stress. The current method has the following capabilities:

1. The interface can be tracked through large distortions.

2. Accurate shock-capturing schemes can be implemented for Cartesian grids and extended in a straightforward manner to incorporate the presence of the moving interfaces.

3. Boundary conditions are developed for the 1D uniaxial strain case and 2D plane strain case and these are applied at the exact locations of the boundaries.

4. Different regions of the boundaries can have different boundary conditions, i.e. the material-material and material-void boundary conditions. These are applied at the interface points identified to lie in regions where the interfaces are in contact and where the interface is exposed to void respectively. These boundary conditions are physically dictated or numerical boundary conditions. The suitability of the set of boundary conditions is determined based on numerical experimentation. The singularity resulting from an abrupt transition from a material-material to material- void boundary condition at the interfaces is handled well.

A Moving-grid Method for Fluid-structure Interaction: Soft Contact Lens

A soft contact lens is spherical in projected shape and has a diameter around 12 to 14 mm. The optical power of the lens determines the lens posterior central radius (base curve radius) and its thickness. Commonly used base curve radii range from 7.5 to 9.0 mm. Soft contact lenses are made of hydrophilic polymers that have an elastic modulus varying with water content. For example the "1-Day Acuvue" lens by Vistakon contains 58% of water and has an elastic modulus of 0.36 Mpa [WSB98]. A typical lens weighs about 10 mg. When placed on the eye, a contact lens is separated from the eye surface by a thin tear film. The thickness of the tear film beneath the lens is around $10\mu m$. So, the aspect ratio between the lens diameter and tear film height is very large, of the order of 1000. Figure 6(a) illustrates the lens-eye profile. An eye-blink creates a force on the contact lens that causes the contact lens to move and deform. Since the lens material makes the soft contact lens very flexible, the lens can exhibit complex shape deformation characteristics.

Francois et al. [FSU99] have presented a computational capability to simultaneously model the dynamics of a soft contact lens and fluid dynamics of the tear film flow. In the present model, the deformable contact lens is considered to be an elastic membrane. A schematic of the computational model is presented in Figure 6(b). Specifically, the main features of their model can be summarized as follows: (1) the tear film is considered to be a single layer, Newtonian fluid governed by the Navier-Stokes equations; (2) the soft contact

lens is modeled as an elastic membrane whose tension is regulated by the membrane thickness; (3) the lens is fixed at the edge; (4) the ambient pressure variation is responsible for the lens movement and deformation; (5) the lens structural dynamics and the tear film are modeled as a coupled system so that both the lens and the tear film characteristics, and their interaction, can be investigated simultaneously; (6) the lens thickness is of variable profile based on typical commercial design.

Governing Equations of Tear Fluid and Contact Lens

The governing equation of the soft contact lens considered is the equilibrium equation of an elastic massless membrane in 2D [SS95, SURS96]. Figure 7 illustrates an elastic membrane restrained at its both extremities. Here only the equilibrium lens equation in the normal direction is considered:

$$-\frac{\Delta P}{\gamma} = \frac{P - P_a}{\gamma} = \left[\frac{d^2y}{dx^2} \left(1 + \left(\frac{dy}{dx} \right)^2 \right)^{-\frac{3}{2}} \right] \tag{1}$$

where P_a is the outside or applied pressure, P is the pressure in the tear film beneath the lens, γ is the lens tension, which is taken to be proportional to the product of the lens elastic modulus and the lens thickness and (x, y) are the space coordinates. The fluid flow computation is based on a well-established pressure-correction type finite volume solver of the Navier-Stokes equations, in body-fitted curvilinear coordinates, as detailed in [Shy94, SURS96, SS97]. Since the initial structure configuration and associated body-fitted grid do not correspond to an equilibrium configuration a moving grid procedure is employed [SURS96, SS95, SS96] wherein the grid is continuously updated during the course of computation, in response to the shape change of the lens. Three key information items are required to facilitate the moving grid technique, namely,

1. Kinematics conditions apply at the interface (moving boundaries).
2. The geometric conservation law is invoked [SURS96] to estimate the Jacobian of term to enforce volume conservation.
3. The contravariant velocity components and Cartesian velocity components at the boundary are computed to enforce mass conservation.

Results and Discussion

Results of the computations for three configurations with tear film aspect ratios (ratio of the horizontal projected length between the center and the pinned end point to the tear film height at the pinned location) of 10, 100, and 1000 are presented. It should be noted that, while under practical wearing conditions the aspect ratio of the tear film is around 1000, we have treated this aspect as a parameter to gain a more comprehensive understanding of the physics. The computational domain and boundary conditions used are presented in Figure 6(b). The overall geometry including lens, tear film, and cornea and the variable lens thickness profile is illustrated in Figure 8. An externally imposed time-dependent pressure, modeling eye blinking process, is represented in Figure 9. Figure 10 shows the maximum lens deflections

normalized by the initial tear film height at the lens center, for the three cases with variable thickness, in response to the imposed pressure variation. Figure 11 presents the maximum pressure difference inside the tear film normalized by the applied pressure oscillation versus time. From Figures 10 and 11, it is clear that the pressure variations and the lens deformation are correlated with each other. Accordingly, as shown in Figure 12, the tear flow rate is influenced by such a correlation.

Francois et al. [FSU99] have also discussed the fluid physics of soft contact lens. First, the tear fluid velocity, responding to the lens deformation, increases from the central region toward the end of the lens. Second, the pressure gradient does not develop only along the direction of the lens, as suggested by a typical thin film approximation. The reason is that the lens movement is not slow and the tear film is not a simple parallel viscous flow. A straightforward application of the thin film theory without due consideration of the lens movement can introduce large error in the analysis. Under the present condition, as illustrated in Figure 13, the Reynolds number increases as the aspect ratio increases, from negligibly small to about 100. These observations indicate that common practices in the literature, with either a straightforward application of the thin film theory, without an explicit consideration of the lens movement, or a direct account of the structure dynamics with an assumed pressure field are unsatisfactory.

Concluding Remarks

We have described the development of numerical techniques based on both fixed and moving grid to treat sharp interface for the simulation of moving boundary problems. Examples arising from fast transient multi-material impact dynamics and soft contact lens are used to illustrate the main features of each method. For the fixed grid method, computations of the deformation process are carried to large distortions while the interfaces travel through the mesh in a stable and robust manner. Such a technique has also been successfully applied to treat problems arising from crystal growth [UMS99]. On the other hand, if the detail of the interface characteristics can be smeared out, then a simpler treatment involving the immersed boundary treatment [Pes77, UT92, UKSTST97, KUSTST98] can be highly effective. This approach has tackled a variety of problems, especially for those related to multiphase and cellular dynamics. For the moving grid method, the implications of the lens tension variations on the lens response and the nonlinear interaction between the fluid flow and the soft contact lens are demonstrated. When the interface does not exhibit substantial deformation, the moving grid method can be highly effective. It can also be robust in terms of the size of the time steps. This approach has been successfully applied to handle fluid-structure interaction problems with high Reynolds numbers, including the effect of turbulence and laminar-to-turbulent transition [SS95, SS96, SJS97, HFS$^+$00]. No method is universally superior for treating moving boundary problems. Depending on the nature of the problem and the goal of the computation, an intelligent selection of an appropriate technique can help successfully address the physical and numerical challenges.

Acknowledgements

The research reported has been supported by AFOSR, Eglin AFB, and Johnson & Johnson.

References

[AP91]Nasser Ashgriz and J.Y. Poo. Flair - fux line-segment model for advection and interface reconstruction. *Journal of Computational Physics*, 93(2):449–468, April 1991.

[BKZ92]J.U. Brackbill, Douglas B. Kothe, and C. Zemach. A continuum method for modeling surface tension. *Journal of Computational Physics*, 100(2):335–354, June 1992.

[Cra84]John Crank. *Free and Moving Boundary Problems*. Oxford University Press, New York, 1984.

[DS85]A.J. DeGregoria and L.W. Schwartz. Finger breakup in hele-shaw cells. *Physics of Fluids*, 28:2313–2314, 1985.

[FR89]J.M. Floryan and Henning Rasmussen. Numerical methods for viscous flows with moving boundaries. *Applied Mechanics Reviews*, 42(12):323–340, 1989.

[FSU99]Marianne Francois, Wei Shyy, and HS Udaykumar. Computational mechanics of soft contact lenses. Bulletin of the American Physical Society, 52nd Annual Meeting of the Division of Fluid Dynamics, November 1999.

[FZP+93]J. Fukai, Z. Zhao, Dimos Poulikakos, Constantine M. Megaridis, and O. Miyatake. Modeling of the deformation of a liquid droplet impinging upon a flat surface. *Physics of Fluids*, 5:2588–2599, 1993.

[GGL+88]James Glimm, J Grove, B Lindquist, OA McBryan, and G Tryggvason. The bifurcation of tracked scalar waves. *SIAM J. Sci. Stat. Comput.*, 9:61–79, 1988.

[HEOC97]Ami Harten, Bjorn Engquist, Stanley Osher, and Sukumar R. Chakravarthy. Uniformly high-order accurate essentially non-oscillatory schemes, iii. *Journal of Computational Physics*, 131:3–47, 1997.

[HFS+00]Xiong He, Carlos Fuentes, Wei Shyy, Yongsheng Lian, and Bruce Carroll. Computation of transitional flows around an airfoil with a movable flap. AIAA Fluids 2000 and Exhibit, Paper no. AIAA-2000-2240, June 2000.

[HLS94]Thomas Y. Hou, John S. Lowengrub, and Michael J. Shelley. Removing the stiffness from interfacial flows with surface tension. *Journal of Computational Physics*, 114:312–338, 1994.

[HN81]CW Hirt and BD Nichols. Volume of fluid (vof) method for the dynamics of free boundaries. *Journal of Computational Physics*, 39:201–225, 1981.

[KUSTST98]Heng-Chuan Kan, HS Udaykumar, Wei Shyy, and Roger Tran-Son-Tay. Hydrodynamics of a compound drop with application to leukocyte modeling. *Physics of Fluids*, 10(4):760–774, April 1998.

[Mey94]Marc A. Meyers. *Dynamics Behavior of Materials*. John Wiley & Sons Inc., New York, 1994.

[Pes77]Charles S Peskin. Numerical analysis of blood flow in the heart. *Journal of Computational Physics*, 25:220–252, 1977.

[Shy94]Wei Shyy. *Computational Modeling for Fluid Flow and Interfacial Transport*. Elsevier Science Publishers B.V., Amsterdam, The Netherlands, 1994.

[SJS97]Wei Shyy, David A. Jenkins, and Richard W. Smith. Study of adaptive shape airfoils at low reynolds number in oscillatory flows. *AIAA Journal*, 35:1545–1548, 1997.

[SO88]Chi-Wang Shu and Stanley Osher. Efficient implementation of essentially non-oscillatory shock-capturing schemes. *Journal of Computational Physics*, 77:439–471, 1988.

[SO89]CW Shu and S Osher. Efficient implementation of essentially non-oscillatory shock-capturing schemes ii. *Journal of Computational Physics*, 83:32–78, 1989.

[SS95]Richard W. Smith and Wei Shyy. Computation of unsteady laminar flow over a flexible two-dimensional membrane wing. *Physics of Fluids*, 7:2175–2184, 1995.

[SS96]Richard W. Smith and Wei Shyy. Computation of aerodynamic coefficients for a flexible membrane airfoil in turbulent flow: A comparison with classical theory. *Physics of Fluids*, 8:3346–3353, 1996.

[SS97]Richard W. Smith and Wei Shyy. Incremental potential flow based membrane wing element. *AIAA Journal*, 35(5):782–788, May 1997.

[SURS96]Wei Shyy, HS Udaykumar, MM Rao, and Richard W. Smith. *Computational Fluid Dynamics with Moving Boundaries*. Taylor and Francis, 1996.

[SZ99]Ruben Scardovelli and Stephane Zaleski. Direct numerical simulation of free-surface and interfacial flow. *Annual Review of Fluid Mechanics*, 31:567–603, 1999.

[UKSTST97]HS Udaykumar, Heng-Chuan Kan, Wei Shyy, and Roger Tran-Son-Tay. Mutiphase dynamics in arbitrary geometries on fixed cartesian grids. *Journal of Computational Physics*, 137:366–405, 1997.

[UMS99]HS Udaykumar, Rajat Mittal, and Wei Shyy. Computation of solid-liquid phase fronts in the sharp interface limit on fixed grids. *Journal of Computational Physics*, 153:535–574, 1999.

[USR96]HS Udaykumar, Wei Shyy, and MM Rao. Elafint - a mixed eulerian-lagrangian method for fluid flows with complex and moving boundaries. *Int. J. Numer. Meths. Fluids*, 22:691–704, 1996.

[UT92]Salih O. Unverdi and Gretar Tryggvason. A front tracking method for viscous, incompressible, multi-fluid flows. *Journal of Computational Physics*, 100:25–37, 1992.

[UTS$^+$00]HS Udaykumar, L Tran, Wei Shyy, K Vanden, and DM Belk. A combined immersed interface and eno shock capturing method for impact dynamics. AIAA Fluids 2000 and Exhibit, Paper no. AIAA-2000-2664, June 2000.

[WM86]HP Wang and RT McLay. Automatic remeshing scheme for modeling hot forming process. *J. Fluids Engrg.*, 108:465–469, 1986.

[WSB98]G Wilson, JD Schwallie, and RE Bauman. Comparison by contact lens cytology and clinical tests of three contact lens types. *Optometry and Vision Science*, 75(5):323–329, 1998.

[YMUS99]Tao Ye, Rajat Mittal, HS Udaykumar, and Wei Shyy. A cartesian grid method for simulation of viscous incompressible flow with complex immersed boundaries. *Journal of Computational Physics*, 156:209–240, 1999.

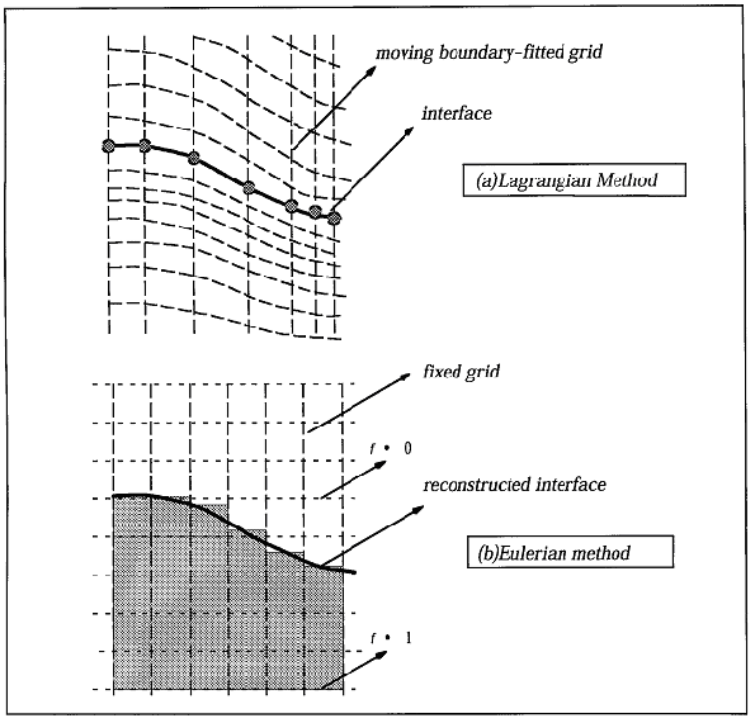

Figure 1: Comparison of Lagrangian and Eulerian methods for interface tracking. (a) Purely Lagrangian method with a moving, boundary conforming grid. (b) Fixed grid Eulerian method with a phase fraction definition of the interface.

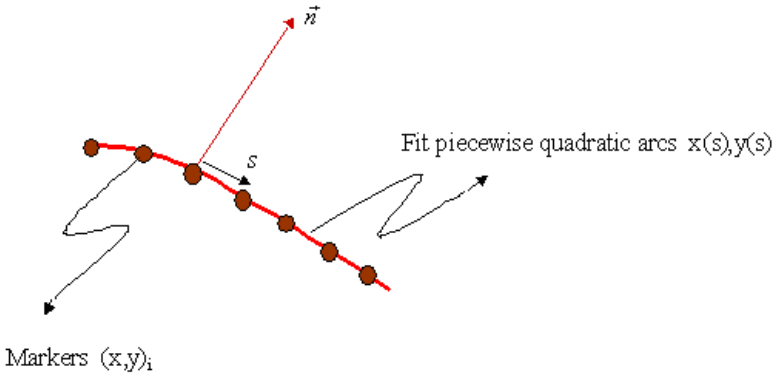

Figure 2: Illustration of interface properties. The normal to the interface and arclength coordinate are shown.

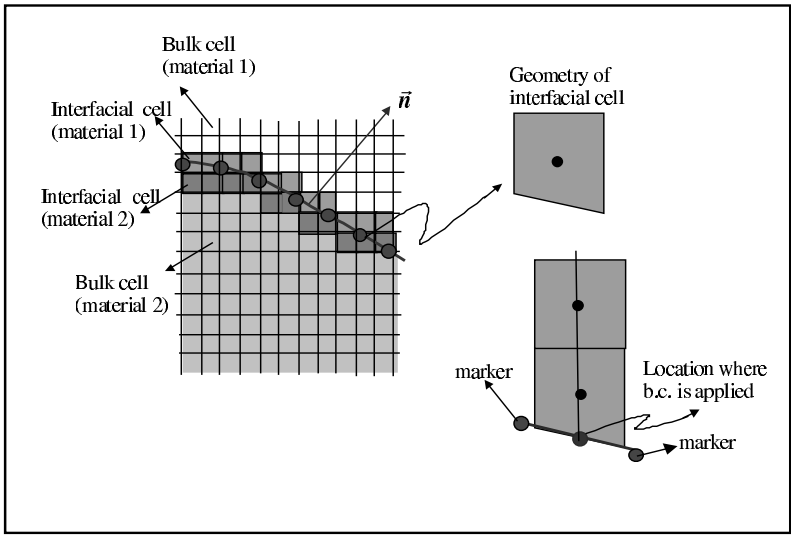

Figure 3: Interfacial cell and bulk cell classification on a grid. With interface passing through it. Also shown are interfacial cell properties.

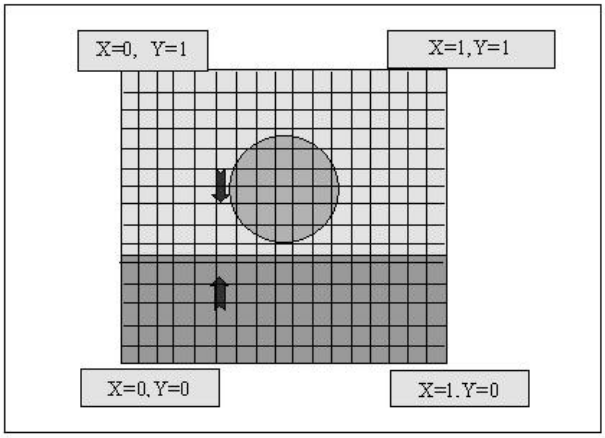

Figure 4: Impact of two objects in the 2D case. A plane strain problem is solved.

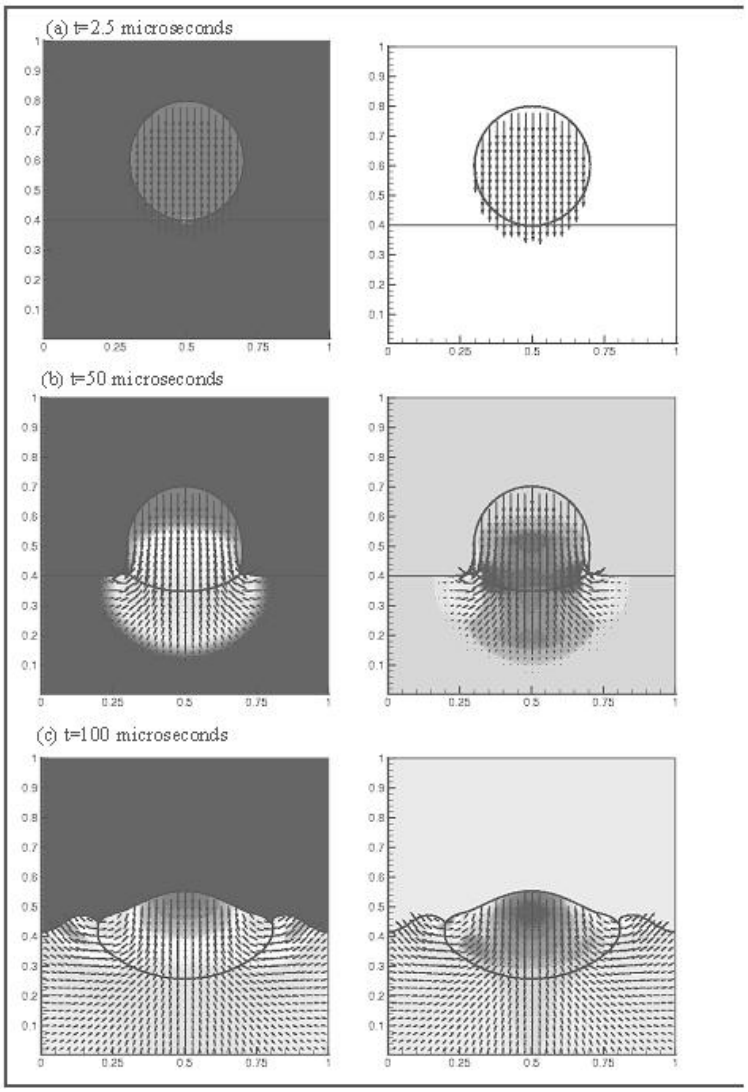

Figure 5: Impact of a cylinder with a planar surface. The cylinder impacts the target with a velocity of $2000 m/s$ directed downward. The figures on left show velocity contours and vectors along with the interface shapes. The time after impact are indicated alongside the figures. The figures on the right show stress contours.

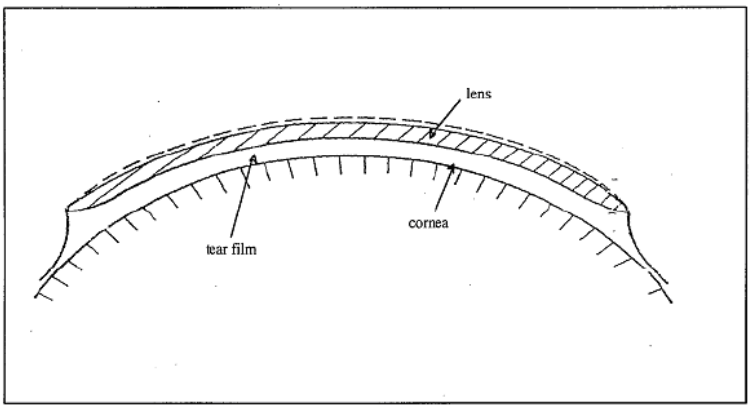

(a) Experimental observation (adopted after Hayashi 1977)

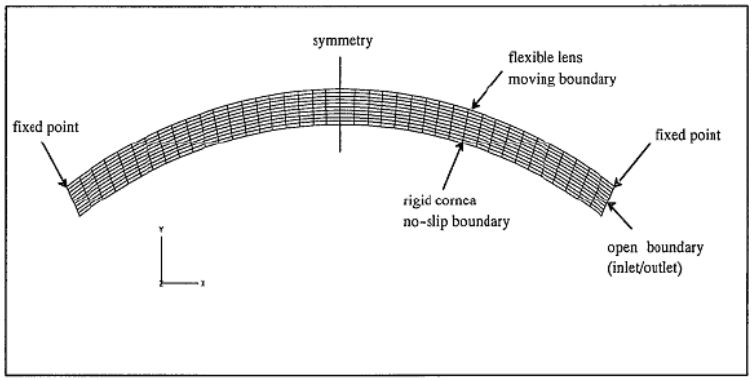

(b) Grid and boundary conditions of the computational model

Figure 6: Schematic of contact lens and computational model.

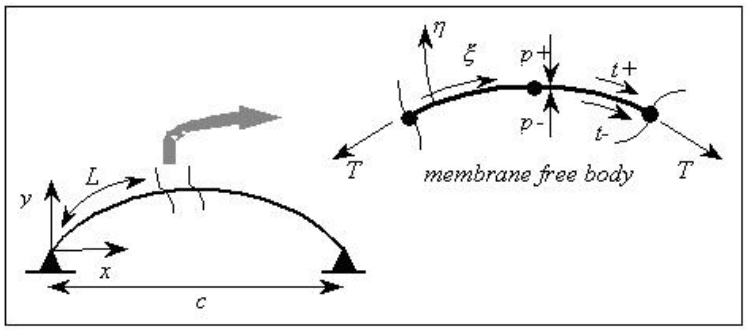

Figure 7: End constrained elastic structure.

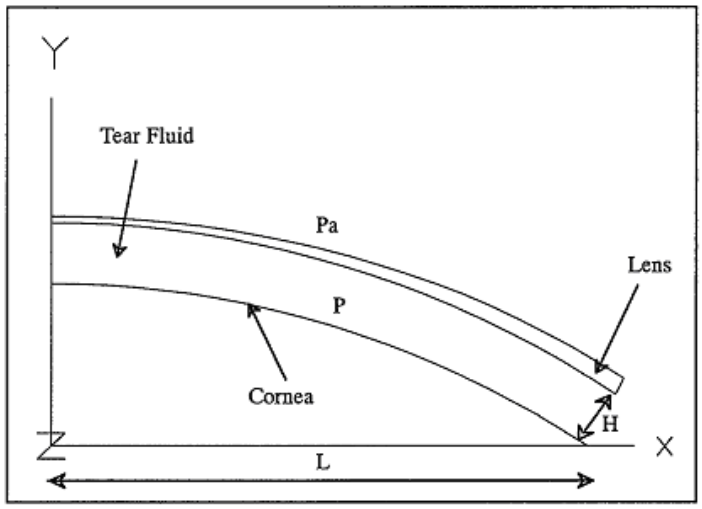

(a) Variable thickness lens (γ variable)

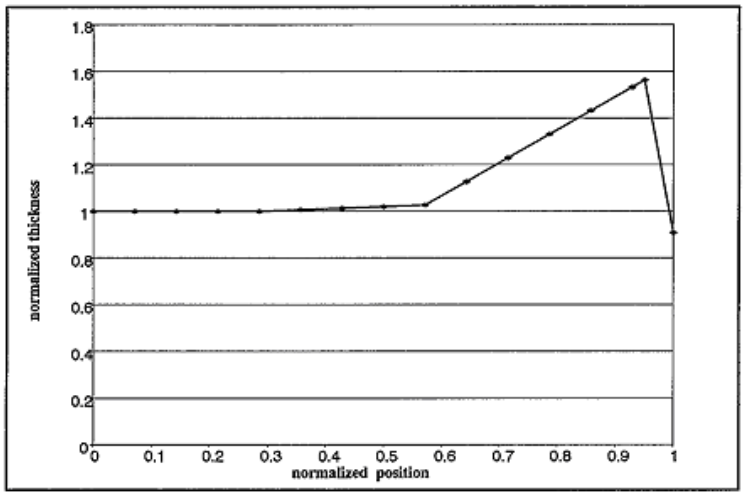

(b) Profile of the variable thickness lens
(0 and 1 indicate, respectively, the center and the end of the lens)

Figure 8: Schematic of the contact lens model and thickness profile.

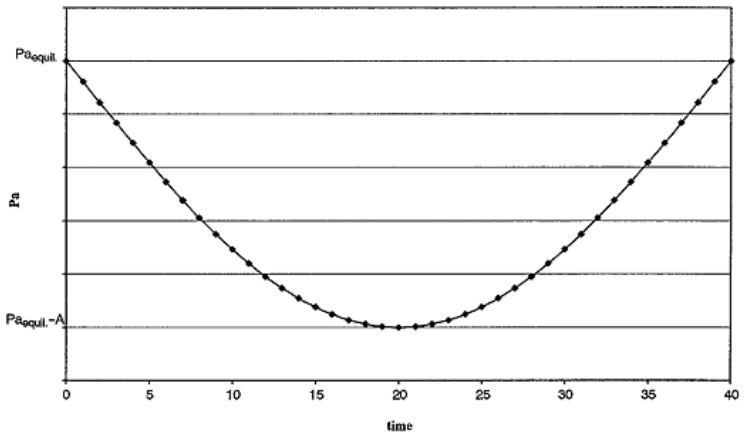

Figure 9: Time History of the applied external pressure $P_a = P_{a_{equil}} - Asin(\frac{\pi}{40}t)$.

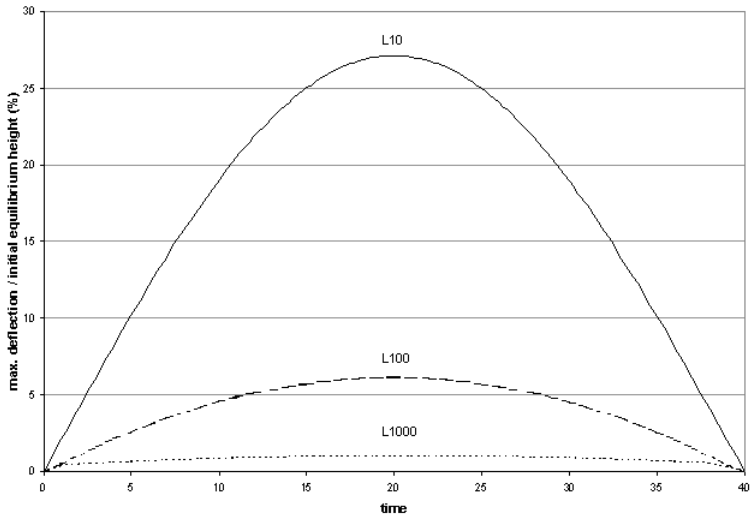

Figure 10: Maximum deflection versus time for three different aspect ratios 10, 100, 1000 with variable thickness.

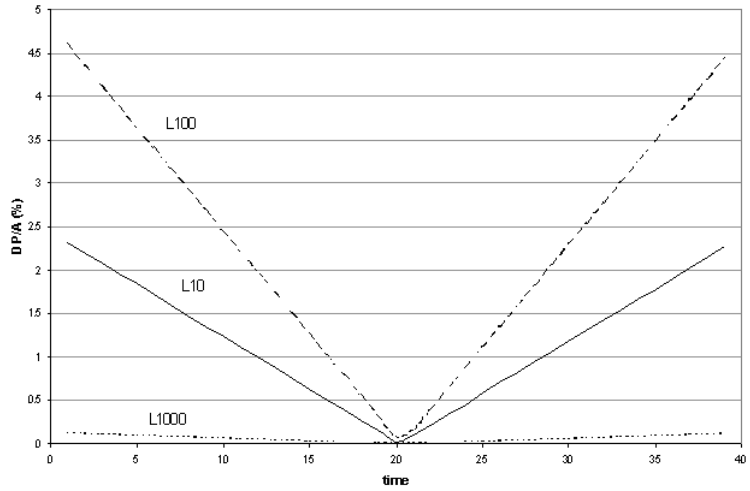

Figure 11: Maximum pressure difference inside the tear film.

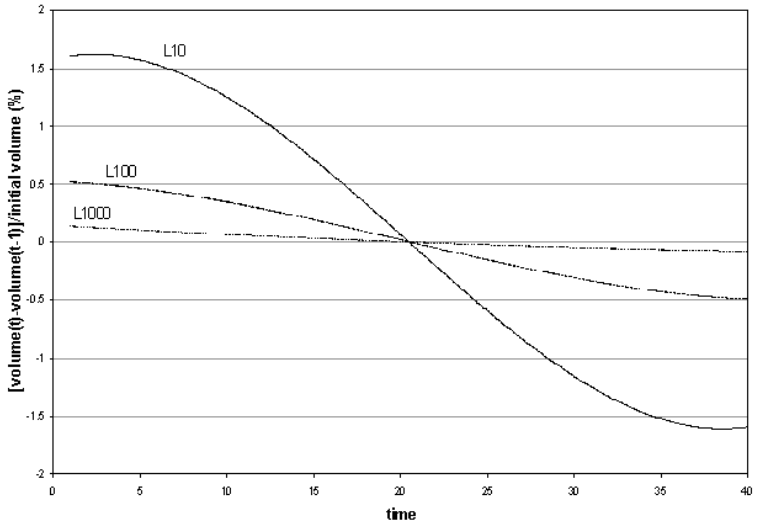

Figure 12: Variation of tear fluid volume going in/out of domain with time.

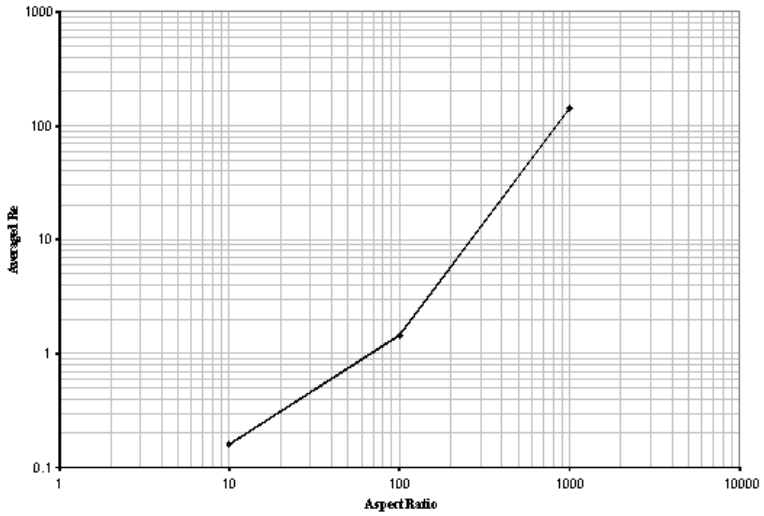

Figure 13: Averaged Reynolds number versus aspect ratio.